

## Therapy of covid complications with terahertz irradiation

© N.T. Bagraev,<sup>1,2</sup> P.A. Golovin,<sup>1</sup> L.E. Klyachkin,<sup>2</sup> A.M. Malyarenko,<sup>2</sup> A.P. Presnukhina,<sup>3</sup> A.S. Reukov,<sup>3</sup>  
V.S. Khromov<sup>2</sup>

<sup>1</sup>Peter the Great Saint-Petersburg Polytechnic University, St. Petersburg, Russia

<sup>2</sup>Ioffe Institute, St. Petersburg, Russia

<sup>3</sup>Almazov National Medical Research Center, St. Petersburg, Russia

e-mail: yellowcat0101@gmail.com

Received January 6, 2022

Revised March 8, 2022

Accepted March 9, 2022

The results of the use of terahertz (THz) irradiation generated by a silicon nanosandwich under conditions of a stabilized source-drain current in the treatment of covid complications are presented. THz irradiation was used in addition to drug therapy for the treatment of patients with COVID-19, which made it possible to reduce the patient's stay in the intensive care unit, reduce the time of patient intubation and stay on mechanical ventilation, and reduce the radiological and pharmacological burden on the patient. An idea was obtained about the resonant response of a living biological tissue to THz irradiation, which made it possible to formulate requirements for irradiation parameters depending on the characteristics of the biological tissue under study. The characteristics of resonant frequencies for the pulmonary alveoli were determined, which made it possible to develop and use the proposed treatment method for the treatment of pneumonia caused by COVID-19.

**Keywords:** silicon nanosandwich, quantum Faraday effect, terahertz irradiation, COVID-19.

DOI: 10.21883/TP.2022.07.54471.7-22

### Introduction

In recent years, material and related nanostructure research demonstrated the presence of macroscopic quantum effects at high temperatures up to room temperature [1–4]. Opportunity to observe these effects arises due to neutralization of electron-electron interaction on edge nanostructure channels due to which the following effects occur: Shubnikov–de Haas high-temperature oscillations, De Haas–van Alphen oscillations, quantum Hall resistance ladder and longitudinal quantum conductivity ladder [1–4]. These effects were observed in graphene and several related topological insulators and superconductors [5,6], and in 6H–SiC and CdF<sub>2</sub> silicone nanostructures whose edge channels were limited by chains composed of the centers with negative correlation energy [1–4]. It should be noted that neutralization of electron-electron interaction in the edge channel is also observed in cases when they are limited by *d*- or *f*-element chains [7,8]. Coatings containing negative-U dipole centers probably contribute a lot to occurrence of macroscopic quantum phenomena at high temperatures [1–4]. Among these macroscopic quantum phenomena, Faraday quantum effect plays a special role and was found to cause capture of single magnetic flux quanta into edge channels containing single carriers which is the cause of THz and GHz radiation generation depending on the edge channel length [9,10]. It has been shown that amplitude-frequency characteristic control is possible not only by means of varying edge channel parameters, but also by means of inclusion of various microresonator systems [9]. Thus, various versions of compact terahertz

radiation sources have been developed and are widely used in practical medicine [9,10].

It should be noted that THz radiation is becoming more common in the global therapeutic practices [11]. Moreover, the far infrared (IR) and THz bands include radiation with wavelengths from 10 to 1000 μm, respectively, with a frequency from 300 GHz to 30 THz, therefore, a certain frequency or wavelength is usually specified to ensure unique characterization. In addition, combination of GHz, THz and IR radiation is of utmost interest for direct therapeutic treatment of biological tissues because IR radiation may stimulate essential biochemical reactions in the body, and the THz radiation component ensures resonant increase in this effect due to „agitation“ of bonds in protein molecules [2,4,9,11], and GHz modulation influences longitudinal oscillations of DNA-oligonucleotides [4,9]. Selection of THz radiation frequency of silicon nanosandwiches (SNS) allows to meet one of the most important practical molecular biology challenges — search for the most efficient method of identification of short DNA strands. Identification of nucleotide strands known as oligonucleotides is widely used in such applications as genetic testing, forensic medicine and DNA amplification [12]. In addition, THz frequency selection of DNA oligonucleotides is an important step towards introduction of personalized medicine for treatment of serious genetic diseases.

Combinations of IR–THz radiation and THz, GHz modulating frequencies may be implemented by the way equivalent to synchronous detecting principle. The synchronous detecting principle is used in radio engineering for radio wave band where short-wave (high frequency)

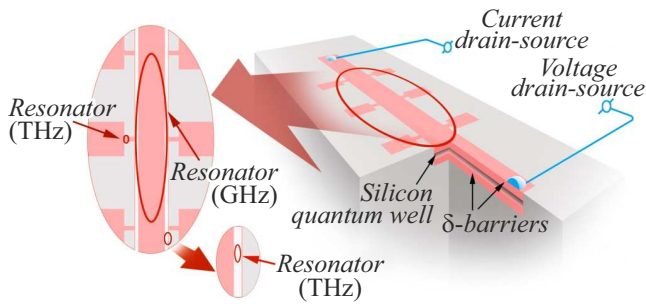


**Figure 1.** Silicon nanostructure used as a modulated THz radiation generator for Covid complication therapy.

radiation is modulated by long-wave (low frequency) radiation, i.e. shorter THz radiation wavelengths will be modulated by long-wave GHz frequencies. From the theoretical perspective, benefit of such research area at the interfaces of disciplines is evident, however, until recently, technological implementation of compact THz radiation sources is not possible. Recently, such sources have been developed on the basis of SNS edge channels [9]. Such device is able to generate 1–700 μm radiation with THz modulation in 40 GHz–3.5 THz band throughout the radiation spectrum [9,10]. This THz radiation source has been already used in various practical medical applications and is highly effective in physiotherapy of a wide disease range, including Covid19 complications.

### 1. Silicone source of THz radiation

This research used SNS which serves as THz emitter for Covid19 complication therapy. SNS is a *p*-type ultra narrow silicon quantum well limited by  $\delta$  barriers, heavily boron-doped ( $5 \cdot 10^{21} \text{ cm}^{-3}$ ) on *n* silicon (100) surface (Figure 1). Boron atoms in  $\delta$  barriers form trigonal dipole centers with negative correlation energy ( $B^+ - B^-$ ) due to negative-U reaction:  $2B^0 \rightarrow B^+ + B^-$  [2,3]. Due to this fact, electron-electron interaction within edge channels is considerably suppressed, and, thus, macroscopic quantum processes, including radiation and THz band receipt, may be carried out at room temperature. Also, preliminary investigations have shown that in stabilized source-drain current conditions, SNS is a source of THz radiation whose characteristics may be controlled both by the flowing current and voltage applied to vertical gates. For this microresonators for various THz- and GHz-band wavelengths are built-in by photolithographic method in the edge channels which are used as real radiation sources (Figure 1).

Using Bruker Vertex 70 Fourier spectrometer, SNS electroluminescence spectra used as THz radiation source for wide therapy range. When longitudinal current  $I_{ds}$  (source–drain) in milliampere range was passed through SNS, far IR- and THz band radiation spectrum was observed [9]. Radiation spectra examples are shown in Figure 2.

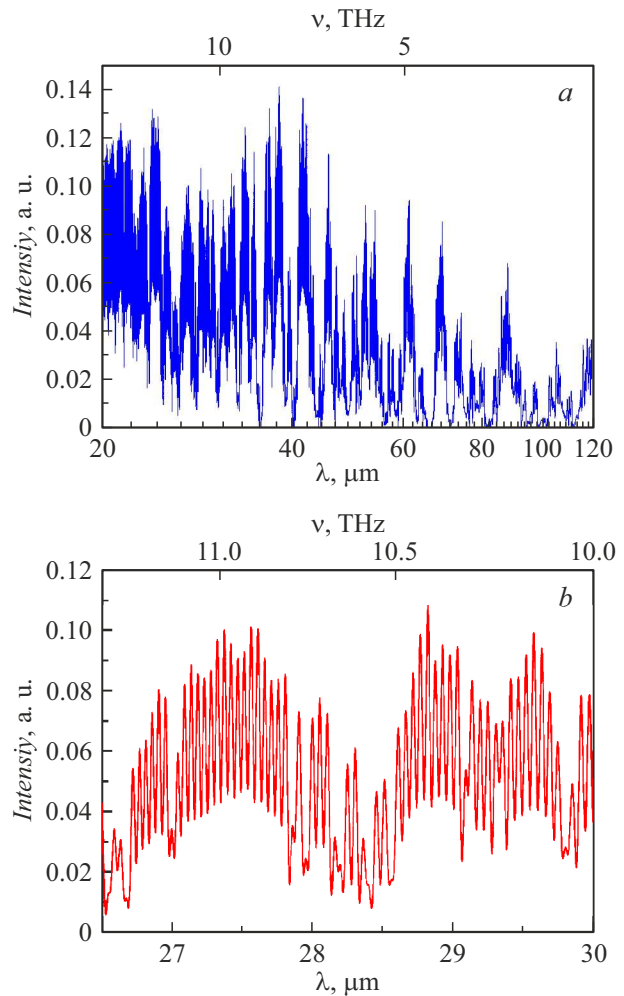


**Figure 2.** Fragments of modulated broadband THz radiation spectrum from SNS demonstrating modulation by frequencies: *a* — 1 THz, *b* — 20 GHz.

THz radiation generation model is offered below in SNS edge channels. The magnetic field dependences of the longitudinal voltage  $U_{xx}$  of SNS [2,3] provides an experimental value of the Aharonov–Bohm (AB) type oscillation period:  $\Delta B = 0.125 \text{ mT}$ , from which a longitudinal size  $l_0$  of the edge channel region, where single carrier interference takes place, can be evaluated:

$$l_0 = \frac{\Phi_0}{\Delta B d_0}, \tag{1}$$

where  $\Phi_0 = h/e$  — is a magnetic flux quantum, and as edge channels width  $d_0$ , value 2.0 nm may be assumed which is specified in [2,3] as a typical distance between the barriers containing dipole boron centers with negative correlation energy which form edge channels limiting the ultra narrow quantum well. Thus,  $l_0 \approx 16 \mu\text{m}$  value is derived. It may be concluded that an edge channel of the studied structure consists of single carrier interference regions taking into account their two-dimensional density defined from Hall measurements —  $3 \cdot 10^{13} \text{ m}^{-2}$ . Actually,

this two-dimensional density corresponds to the distance between carriers (holes) in the edge channel  $\approx 16 \mu\text{m}$ . Thus, each area of edge channel containing a single carrier („pixel“) consists of layers containing boron dipoles and having the size  $S_{\text{pixel}} = 16 \mu\text{m} \times 2.0 \text{ nm}$ , through which the carrier is tunneling; these two layers confine the quantum well core with a width and height of approx 2.0 nm, because in the process of sample boron-doping boron concentration changes at the distances of about 2 nm in accordance with the measurements of the De Haas–van Alphen (dHvA) oscillations [1,3].

It should be noted that the area  $S_{xx}$  of the edge channel between  $xx$ -contacts  $S_{xx} = 2000 \mu\text{m} \times 2.0 \text{ nm} = 4 \cdot 10^{-12} \text{ m}^2$  has  $\sim 125$  single carriers, which corresponds to two-dimensional density  $n_{2D} \approx 3 \cdot 10^{13} \text{ m}^{-2}$ . This value agrees with the values obtained from the measurements of the field dependences of magnetic susceptibility and Hall measurements [1].

The similar regions-pixels exhibit quantum conductivity property [1]. That is why the edge channel can be considered as a ballistic one, wherein each of the pixels can be characterized by the resistance equal to resistance quantum  $h/(e^2)$ . Furthermore, since the electron-electron interaction may be suppressed strongly under high pressures of several hundred GPa at the silicon substrate-negative correlation energy center chains interface as described above, formation of double-length pixels containing a pair of carriers with possible Josephson transition near the pixel interface is possible. The double-length pixels are characterized by the resistance equal to  $h/(4e^2)$ .

Based on the above, the radiation generation process may be assessed. Longitudinal current  $I_{ds}$  flowing through the structure creates magnetic field  $B$ . This field can be evaluated by taking into account that  $I_{ds}$  can form circuits. In the simulated current turn

$$B \approx \mu_0 \frac{I_{ds}}{2r}, \quad (2)$$

where the effective radius  $r$  is correlated by  $r = \sqrt{S/\pi}$  with area  $S$  covered by the circuit.

Thus, the longitudinal current flow causes occurrence of flux  $\Phi = BS$  in area  $S$  and change of flux  $\Delta\Phi$  in the double-length individual pixel area; this process inside it also results in the generation current:

$$I_{gen} = \frac{U_{xy}}{R_{\text{pixel}}}, \quad (3)$$

where  $R_{\text{pixel}} = h/(4e^2)$  for the double-length pixel, and  $U_{xy}$  is voltage measured at  $xy$ -contacts of the structure depending on  $I_{ds}$ . Such measurement give  $U_{xy} = 3.5 \Omega \cdot I_{ds}$ .

The emitted radiation frequency can be calculated using the Faraday formula:

$$I_{gen} = \frac{\Delta E}{\Delta\Phi} = \frac{h\nu}{\Delta\Phi}. \quad (4)$$

The change of the flux in the individual double-length pixel

$$\Delta\Phi = \frac{m}{N} \Phi_0 \quad (5)$$

depends on their number  $N = S/(2S_{\text{pixel}})$  inside area  $S$  and the number of  $m$  of the flux quanta  $\Phi_0 = \frac{h}{2e}$ , which are captured on  $N$  pixels;  $m$  accepts values  $1, 2, \dots, \frac{BS}{h/(2e)}$ , the latter corresponds to uniform population. The frequency is equal to

$$\nu = I_{gen} \cdot \frac{m}{N} \cdot \frac{1}{2e}. \quad (6)$$

When  $I_{ds} = 30 \text{ mA}$ , id circuit  $I_{ds}$  cover the edge channel area

$$S_{ds} = 4700 \mu\text{m} \times 2.0 \text{ nm} = 9.4 \cdot 10^{-12} \text{ m}^2,$$

then frequency with minimum current change corresponds to 9.3 GHz. If circuit  $I_{ds}$  covers the pixel area

$$S_{\text{device}} = 16 \mu\text{m} \times 2.0 \text{ nm} = 32 \cdot 10^{-15} \text{ m}^2,$$

then, in these conditions, frequency with minimum current change corresponds to 2.8 GHz. The obtained values well agree with the frequency values which are found in detail study of the obtained electroluminescence spectra [9].

Thus, in the mid- (up to  $27 \mu\text{m}$ ) and far- (up to  $333 \mu\text{m}$ ) IR wavelength bands, the spectra have modulations. The Fabry-Perot resonator model correlates the distance  $\Delta\nu$  between the adjacent peaks to the geometrical length  $L_0$  of the resonator:

$$\Delta\nu = \frac{c}{2L_0n}, \quad (7)$$

where  $c$  is the speed of light in vacuum,  $n$  is the refraction index of the medium. The found features correspond to the values of modulation frequencies  $\Delta\nu = 9.3 \text{ GHz}$  and  $2.8 \text{ THz}$  [9].

Modulation frequencies 1 THz and 20 GHz (Figure 2) are fundamental herein. Due to the fact that THz band radiation is completely suppressed by skin and its energy is spent for epithelium tissue warming, initial use of THz radiation at high frequencies was not possible for solution of the existing problems. On the other hand, the use of broadband radiation spectrum modulated in the gigahertz band makes it possible to achieve a penetration effect which causes resonant processes in human biological tissues, in particular lung alveoli tussues which, in turn, ensures efficient pneumonia therapy. Frequencies from 2.2 to 3.4 THz were used as carriers herein. For this, 1.0 THz and 20 GHz frequencies were used as modulation frequencies. In the first case, the desired modulation frequency was achieved using variation of the individual gate voltage applied to pixels, and in the second case — when using 2 mm microresonators integrated into SNS edge channels by silicone photolithographic method (Figure 1, 2).

This selection of modulation frequencies has been determined by the structure of the pulmonary bronchi system some parts of which represent a self-ordered microresonator

system. Thus, the bronchial tree consists of bronchioles which represent microresonators with frequencies corresponding to the range near 20 GHz. Modulating frequencies corresponding to alveoli-based microresonators are of utmost interest. This range covering the value about 1 THz corresponds to this objective, i.e. the effect of this modulating frequency makes it possible to stimulate oxygen penetration into red blood cells in arterial channels with subsequent transport. The foregoing defines the importance of the current research which studied the resonant effect of the modulated THz radiation on the self-ordered microresonator system of the bronchial tree in order to stimulate oxygen transport from external environment.

## 2. THz radiation in pulmonology

Development of pulmonary complications will aggravate the state of cardiac surgery patient, requires additional treatment and diagnostic measures, increases pharmacological load, increases inpatient stay time and may lead to lethal outcome. Therefore, the Almazov National Medical Research Center (Saint Petersburg) has analysed the opportunity and proved the efficiency of THz radiation generated by „IK-Dipol“ for pulmonary pathology treatment as a result of hospital-acquired pneumonia and ventilator-associated pneumonia in patient at early post cardiac surgery stages.

Observational nonconcurrent non-blind comparative study with pseudocontrol („main group–control group“) was carried out on the basis of a cardiovascular surgery intensive care unit where coronary artery bypass surgery and/or mitral valve replacement patients were kept. The study included patients with advanced complications in the form of focal pulmonary infiltrates (community-acquired pneumonia and ventilator-associated pneumonia). Two groups were subdivided: group in which together with medication therapy THz radiation exposure of acupuncture point Dabao was involved using „IK-Dipol“ (RP 21), and control group administered with standard treatment.

Comparative analysis of „IK-Dipol“ performance for treatment of pneumonia of various origin is shown in [9]. It was shown that early (during the first days) use of THz radiation made it possible to reduce the patient's stay time in the intensive care unit by 4–8 days; reduce radiological and pharmacological load on the patient; reduce intubation time and mechanical ventilation time by 4–8 days; increase the favorable prognosis opportunities in patients with risk factors; start intensive care measures 4–8 days earlier.

As typical clinical examples of efficient THz radiation exposure in Figure 3 shows the behavior of key blood indicators in pneumonia treatment using THz radiation together with standard medication methods in coronary heart disease, coronary artery atherosclerosis, stenocardia and idiopathic hypertension patients. The patient received sternotomy, coronary artery bypass, vein transplantation to obtuse marginal artery, diagonal artery, right coronary artery,

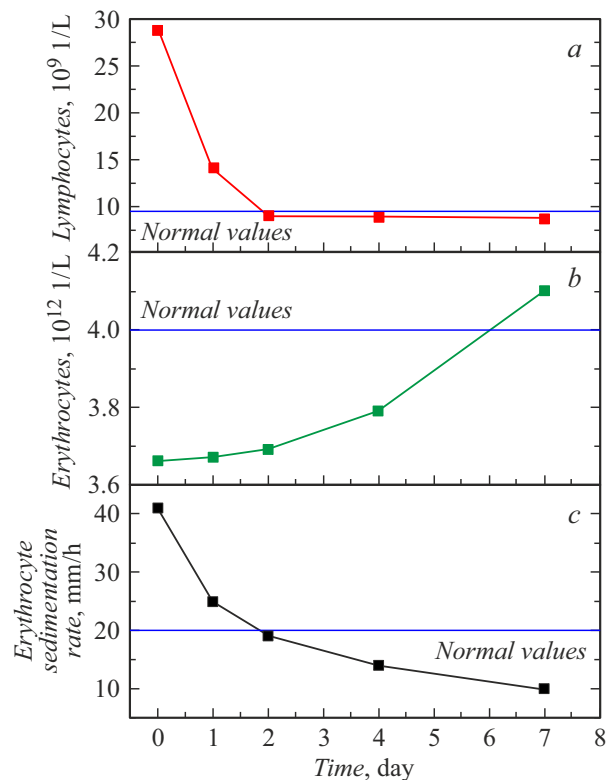


**Figure 3.** A typical example of changes in key blood indicators in pneumonia treatment using THz irradiation together with standard medication technique is: *a* — white blood cells, *b* — red blood cells, *c* — erythrocyte sedimentation rate.

with artificial blood flow and blood cardioplegia. Post-surgery progress was very severe with cardiovascular and respiratory insufficiency, metabolic disorder, bilateral lower lobe pneumonia, septicemic condition. Addition of THz radiation using „IK-Dipol“ to the medication therapy made it possible to remove mechanical ventilation after 5 days and to bring the key blood indicators to normal condition within 8 days.

## 3. Using THz radiation in novel coronavirus infection complicated by pneumonia

This study included 12 patients of age 44 to 67 with U07.1 + J12.8 who were dynamically observed in the early rehabilitation period in hospital. Patients, Saint Petersburg based, were hospitalized in the municipal medical facilities with signs of respiratory insufficiency, dry cough, weakness and hyperthermia. After hospitalization, „COVID-19 virus was identified“ and confirmed. According to computerized tomography (CT), clinical-biochemical blood tests (with v markers), the diagnosis was updated and supplemented by community-acquired bilateral multisegmental pneumonia and I degree respiratory insufficiency as complications of the basic disease.

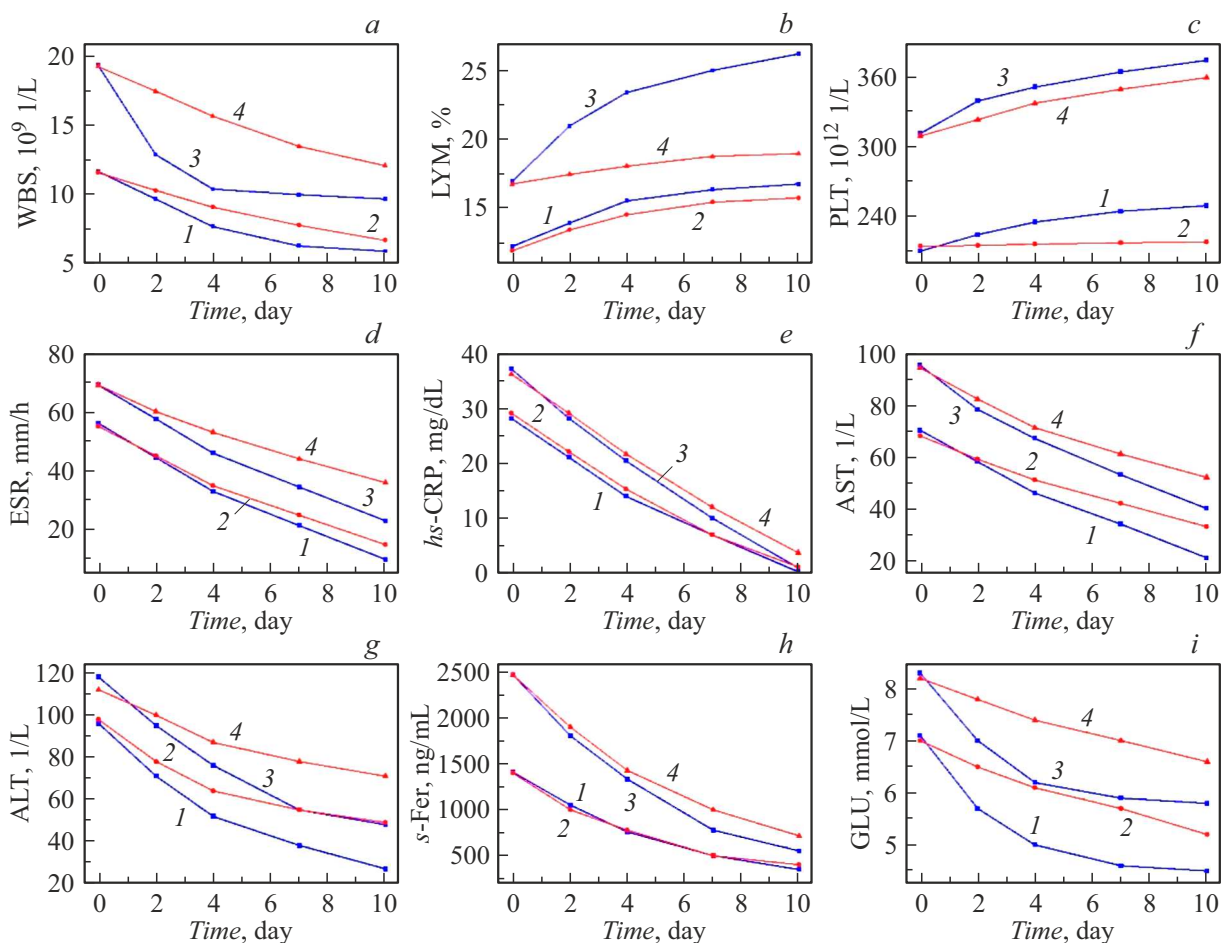


**Figure 4.** Clinical blood indicator (minimum and maximum per group) behavior in patients from the main group who received additional THz physiotherapy and control group patients: 1, 3 — main group; 2, 4 — control group.

The patients examined according to their age, sex, main diagnosis, complications and clinical symptoms were divided into two groups compared by these parameters: main group and control group. Patients of both groups received antibacterial, anti-inflammatory, symptomatic, antiviral and gastroprotective therapy. In addition to drug therapy in the early rehabilitation period, patient from the main group received a course of daily THz therapy using „IK-Dipol“ including 10–12 procedures. Patients in both groups consisting of 6 patients (3 men and 3 women) were hospitalized 3–5 days after deterioration in condition. They have no thyroid disorders or changes in past medical history which are typical of this pathology and are detected during examination. The main concurrent diseases in the group included degenerative-dystrophic spine diseases without clinical symptoms requiring medication treatment. All patients had no bad habits. According to CT, all examined patients had multiple wide irregular-shaped confluent focal infiltrations known as „ground-glass opacity“ in all segments of both lungs. The total damaged area exceeded 50%. Clinical and laboratory blood data are shown in Figure 4.

The indications for THz irradiation in the early rehabilitation period included the absence of (stabilization) clinical deterioration, improvement of clinical and laboratory blood and urea indicators. Assessment of such physiological parameters as patients' appetite, sleep, diuresis and defecation was also taken into consideration. The following subjective symptoms were also considered: mood, weakness, headaches, dizziness and performance. Subjective symptoms were assessed using Robson ten-point scale (ascending with increase of the value). Dynamics of such subjective symptoms for patients of both groups is shown in Figure 5.

During THz therapy, acupuncture point temperature control test was used which is successfully used for ventilator-associated pneumonia (VAP) treatment in cardiac surgery patients. Using contactless IR thermometer, skin surface temperature is measured in the multiple representative acupuncture point epicenter projection which allows to make a right selection of irradiation zone using „IK-Dipol“ for therapy performance improvement.

During the study, it has been detected that temperature indicators of thyroid anatomic structures are important

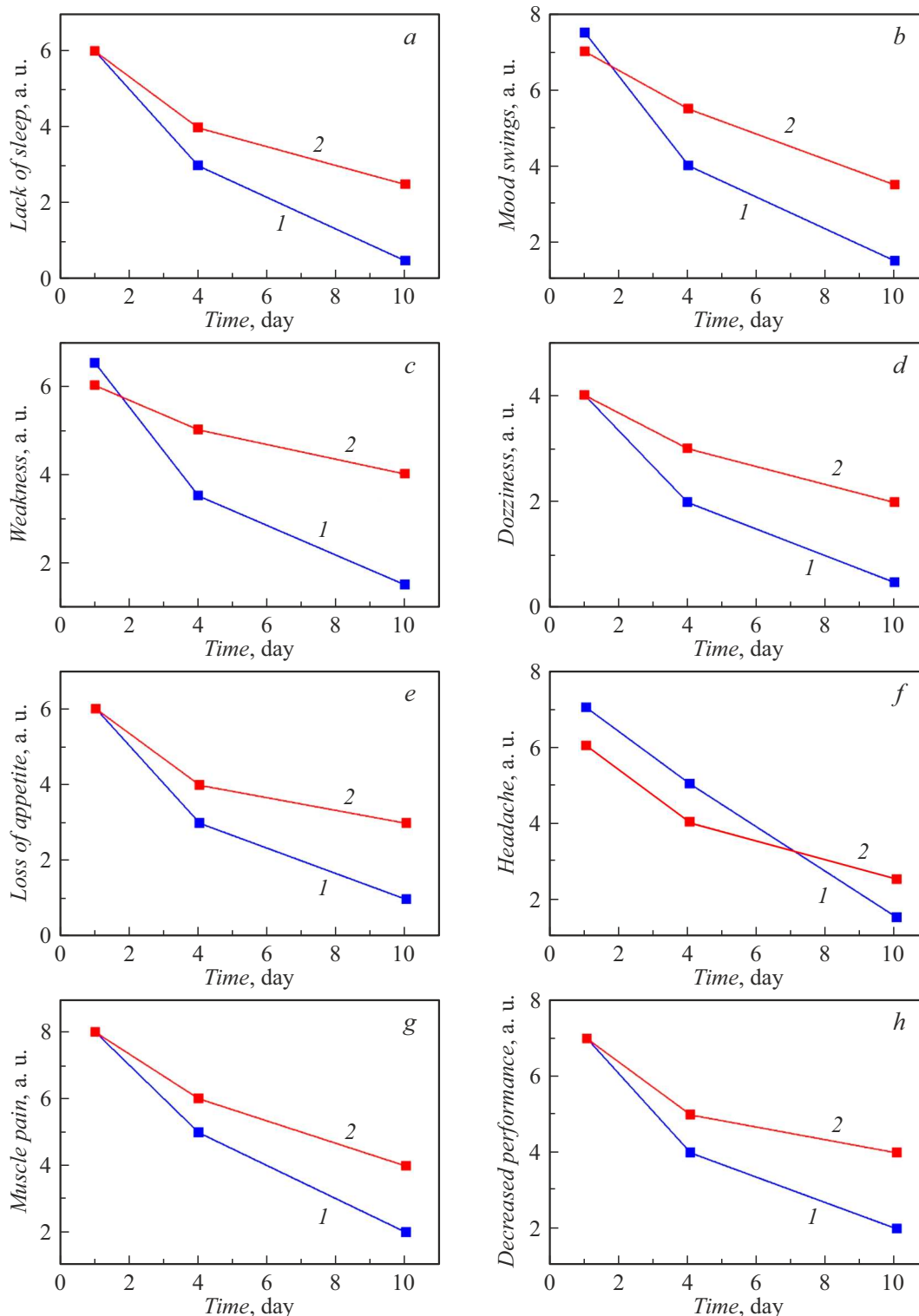


**Figure 5.** Average subjective symptom assessment behavior in patients of both groups: 1 — main group, 2 — control group.

for the assessment of Covid complication progress and shall serve as a reference for THz irradiation procedures in protracted treatment. underarm temperature shall be measured on both sides taking into account the highest readings.

According to CT, both studied groups showed regular pathological process progress with favorable dynamics. However, THz irradiation occurred to be an important additional factor of favorable outcome of Covid infection complicated by pneumonia. Considering various drug

therapy and intensive care versions and areas, THz irradiation reduces side effects and facilitates quick recovery at the early rehabilitation stage. By the end of THz therapy course, clinical and biochemical blood indicators almost in all patients with myasthenia gravis (MG) were within normal limits.

The foregoing indicates high potential of THz radiation used for Covid-caused pneumonia therapy. Since Covid causes atypical pneumonia with prevailing alveoli damage, THz radiation exposure may stimulate protein transport in cell, activate cell protective mechanisms and prevent virion attachment to a cell receptor [9]. In addition, THz irradiation causes spin-dependent oxygen capture by iron ions in haem, facilitates oxygen transport and corresponding blood saturation with oxygen (scarlet blood).

The results were obtained by fluorescent flow cytometry using Sysmex XN-1000 modular automatic blood analyzer.

## Conclusion

The foregoing shows the potential of THz irradiation used in medical purposes both for therapy and diagnostics of various pathologies. It has been shown that modulated THz irradiation may be also used for the development of medical equipment for special therapy and prevention of various diseases, since the great majority of essential biochemical reactions in the body are probably enhanced by optical pumping in this spectral band. „IK-Dipol“ designed to implement these ideas generates modulated THz-irradiation in 1–700  $\mu\text{m}$  band with THz modulation from 20 GHz to 1.5 THz. The device was designed using our latest silicon planar nanotechnology achievements. This technique has a potential for development of a new innovative area — personalized medicine. Personalized medicine will be based on characteristic lengths of biological compounds and potential varying of the emitter spectrum depending on pathology and specific factors of each individual patient.

## Compliance with ethical standards

Informed voluntary consent was obtained from all participants involved in the study.

## Conflict of interest

The authors declare that they have no conflict of interest.

## References

- [1] N.T. Bagraev, V.Yu. Grigoryev, L.E. Klyachkin, A.M. Malyarenko, V.A. Mashkov, V.V. Romanov. *Semiconductors*, **50** (8), 1025 (2016). DOI: 10.1134/S1063782616080273
- [2] N.T. Bagraev, L.E. Klyachkin, A.M. Malyarenko, A.L. Chernev, A.K. Emel'yanov, M.V. Dubina. *Semiconductors*, **50** (9), 1208 (2016). DOI: 10.1134/S1063782616090037
- [3] N.T. Bagraev, V.Yu. Grigoryev, L.E. Klyachkin, A.M. Malyarenko, V.A. Mashkov, N.I. Rul. *Low Temperature Physics/Fizika Nizkikh Temperatur*, **43**, 132 (2017). DOI: 10.1063/1.4974190
- [4] K.B. Taranets, M.A. Fomin, L.E. Klyachkin, A.M. Malyarenko, N.T. Bagraev. *J. Appl. Phys.*, **125** (22), 225702 (2019). DOI: 10.1063/1.5083805
- [5] K.S. Novoselov, Z. Jiang, Y. Zhang, S.V. Morozov, H.L. Stormer. *Science*, **315** (5817), 1379 (2007). DOI: 10.1126/science.1137201
- [6] M.Z. Hasan, C.L. Kane. *Rev. Modern Phys.*, **82** (4), 3045 (2010). DOI: 10.1103/RevModPhys.82.3045
- [7] J. Klinovaja, P. Stano, A. Yazdani, D. Loss. *Phys. Rev. Lett.*, **111** (5), 186805 (2013). DOI: 10.1103/PhysRevLett.111.056802
- [8] A.A. Zyuzin, D. Loss. *Phys. Rev. B: Condens. Matter Mater. Phys.*, **90** (12), 125443 (2014). DOI: 10.1103/PhysRevB.90.125443
- [9] N.T. Bagraev, L.E. Klyachkin, A.M. Malyarenko, B.A. Novikov. *Biotekhnosfera*, **5**, 55 (2015) (in Russian).
- [10] V.V. Kirianova, E.N. Zharova, N.T. Bagraev, A.S. Reukov, S.V. Loginova. *Fizioterapiya. Balneologiya i reabilitatsiya*, **15** (4), 209 (2016) (in Russian). DOI: 10.18821/1681-3456-2016-15-4-209-215
- [11] E. Pickwell, B.E. Cole, A.J. Fitzgerald, M. Pepper, V.P. Wallace. *Phys. Medicine Biology*, **49** (9), 1595 (2004).
- [12] A.L. Chernev, N.T. Bagraev, L.E. Klyachkin, A.K. Emelyanov, M.V. Dubina. *Semiconductors*, **49** (7), 944 (2015). DOI: 10.1134/S1063782615070064